JACS
JOURNAL OF THE AMERICAN CHEMICAL SOCIETY

Article

pubs.acs.org/JACS

How are Radicals (Re)Generated in Photochemical ATRP?

Thomas G. Ribelli, Dominik Konkolewicz, Stefan Bernhard, and Krzysztof Matyjaszewski*

Department of Chemistry, Carnegie Mellon University, 4400 Fifth Ave, Pittsburgh, Pennsylvania 15213, United States

Supporting Information

ABSTRACT: The polymerization mechanism of photochemically mediated Cu-based atom-transfer radical polymerization (ATRP) was investigated using both experimental and kinetic modeling techniques. There are several distinct pathways that can lead to photochemical (re)generation of Cu^{I} activator species or formation of radicals. These (re)generation pathways include direct photochemical reduction of the Cu^{II} complexes by excess free amine moieties and unimolecular reduction of the Cu^{II} complex, similar to activators regenerated by electron-transfer (ARGET) ATRP processes. Another pathway is photochemical radical generation either directly from the alkyl halide, ligand, or via interaction of ligand with either monomer or with alkyl halides. These photochemical radical generation processes are similar to initiators for continuous activator regeneration (ICAR) ATRP processes. A series of model experiments, ATRP reactions, and kinetic simulations were performed to evaluate the contribution of these reactions to the photochemical ATRP process. The results of these studies indicate that the dominant radical (re)generation reaction is the photochemical reduction of Cu^{II} complexes by free amines moieties (from amine containing ligands). The unimolecular reduction of the Cu^{II} deactivator complex is not significant, however, there is some contribution from ICAR ATRP reactions involving the interaction of alkyl halides and ligand, ligand with monomer, and the photochemical cleavage of the alkyl halide. Therefore, the mechanism of photochemically mediated ATRP is consistent with a photochemical ARGET ATRP reaction dominating the radical (re)generation.

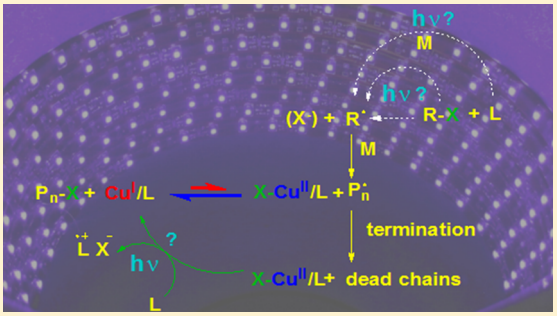

INTRODUCTION

Reversible deactivation radical polymerization (RDRP) techniques have revolutionized the fields of polymer chemistry and materials science over the past two decades. These RDRP methods allow well-controlled polymers with complex architectures to be synthesized as was traditionally possible only with ionic polymerizations.[1] However, RDRP methods have tolerance to functional groups and impurities similar to conventional radical polymerization.[2] The most popular RDRP methods are nitroxide-mediated polymerization (NMP),[3] atom-transfer radical polymerization (ATRP),[4] and reversible addition−fragmentation chain-transfer (RAFT) polymerization.[5] ATRP is one of the most widely used techniques since it can be performed under mild conditions, it is compatible with a wide range of monomers, and it gives excellent control over the polymer structure.[4,6,7]

In ATRP, control over the polymer structure is gained through a catalytic cycle in which a low oxidation state transition-metal catalyst activates an alkyl halide to generate an alkyl radical and an oxidized form of the transition-metal complex.[4,6] This alkyl radical can add several monomer units before being deactivated by the high oxidation state deactivator complex to reform the alkyl halide and the activator complex. This process can be repeated for each alkyl halide over several cycles, allowing the uniform growth of the polymer chains. In the majority of cases, the activator and deactivator complexes are Cu^{I}/L and X-Cu^{II}/L, respectively. However, one limitation of normal ATRP, where alkyl halides and activator complexes are used, is that each radical termination event leads to the irreversible formation of the deactivator complex by the persistent radical effect.[6,8] Therefore, high concentrations of the activator complex were required to maintain an acceptable rate of polymerization throughout the reaction.[4,9] Throughout the remainder of this article, the activator complex will refer to Cu^{I}/L complexes, and the deactivator complex will refer to X-Cu^{II}/L.[4,10]

In recent years, various methods have been developed that allow ATRP to proceed with catalyst concentrations at or below 100 ppm.[9] These low catalyst loadings are possible when the excess deactivator complex is reduced to the activator complex, as indicated in Scheme 1. This reduction can occur by various methods, including: addition of a chemical reducing agent, as is

Scheme 1. ATRP Processes with (Re)Generation Processes

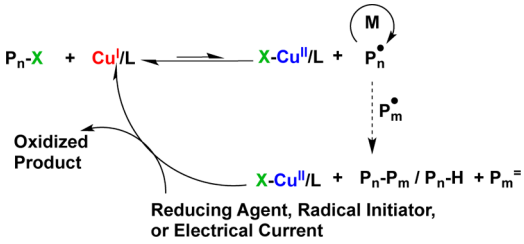

Received: June 25, 2014
Published: September 1, 2014

   dx.doi.org/10.1021/ja506379s | J. Am. Chem. Soc. 2014, 136, 13303−13312

done in activators for continuous activator (re)generation by electron-transfer (ARGET) ATRP,[9] adding an external radical initiator, as is done in initiators for continuous activator (re)generation (ICAR) ATRP,[9] applying a reducing current, as occurs in electrochemically-mediated ATRP,[11] using zerovalent metals or sulfite species as supplemental activators and reducing agents (SARA) in ATRP,[12−15] or to photochemically regenerate activator species.[16−20] Photochemically-mediated ATRP, or photoATRP, processes have received considerable attention recently[16−30] due to the simple preparation, minimal use of additives, and opening the option of using sunlight.[19,20] The option of photochemical and sunlight driven processes has also been used for other RDRP processes such as RAFT[31,32] and the combination of RAFT with iridium or ruthenium catalysts.[23,28,30] Additionally, photochemically controlled organic transformations have received considerable interest in the recent literature.[33−35]

Despite the facile nature of photoATRP, there are several unanswered questions regarding the mechanism of radical formation and activator (re)generation in this photochemical process. These include: do Cu^{I} species participate in photochemical processes?; does the X-Cu^{II}/L deactivator complex undergo unimolecular photochemical reduction?; can Cu^{II} species participate in photochemical redox through other pathways?; and to what extent do the alkyl halide and excess ligand contribute to the photochemical radical generation?

In earlier work, careful measurement of the activation rate of alkyl halides by Cu^{I} species showed negligible dependence on the presence of a UV photon source.[19,22] This indicates that photochemically enhanced alkyl halide activation through excited Cu^{I} complexes is not kinetically significant, in contrast to the iridium-mediated RDRP processes.[21,23,25] Therefore, the Cu-mediated ATRP with typical ligands in the presence of light must proceed by radical formation and activator (re)generation, rather than through enhanced activity of the Cu^{I} complex.

There are several possible ways that the activator and radical species can be regenerated photochemically. One pathway is the unimolecular photochemical cleavage of the Cu^{II}−halogen bond in the excited state to give the Cu^{I}/L activator complex and a halogen radical, as proposed in various reports and shown in the top line of Scheme 2.[16−19] This process would be a hybrid of ICAR and ARGET ATRP, since Cu^{II} is reduced in the presence of light by electron transfer as in ARGET while giving a halogen radical that can initiate new chain, as in ICAR ATRP. An alternative radical (re)generation mechanism has the photoexcited alkyl halide, ligand, or their combined interaction generating radical species which can react with monomer in a photochemical mechanism akin to ICAR ATRP, as shown in lines 2−4 of Scheme 2.[20]

In the case of the alkyl halide, homolytic cleavage of the carbon−halogen bond is anticipated as shown in line 2 of Scheme 2.[36,37] In the case of the photochemical interaction involving the ligand, the nitrogen-centered radical cation is expected to be generated.[37] To conserve both charge and spin, a second molecule must accept this electron. This molecule can be an electron-poor alkene, such as a (meth)acrylate moiety as shown in the third line of Scheme 2.[37] Alternatively, the ligand and alkyl halide can photochemically generate the nitrogen-centered radical cation, an alkyl radical and a halide anion, as shown in line 4 of Scheme 2.[20] A final possibility is that the Cu^{II} complexes in the excited state can react with electron-donating species (e.g., amine), reducing the Cu^{II} species and generating a radical cation species from the ligand, as shown in line 5 of Scheme 2.

It should be noted that all of these photochemical radical (re)generation pathways are parallel pathways. These pathways are shown in Scheme 2. In all cases where the nitrogen-centered radical cation is generated, it rapidly undergoes proton transfer, giving a protonated amine and a carbon-centered radical.[37] This carbon-centered radical can then add to monomer which would result in the formation of a new chain with a positively charged end group. This chain end can either stay as the ionic species or it can become deprotonated to give the neutral amine.

In this work, the kinetic contribution of all pathways shown in Scheme 2 is evaluated for the polymerization of MA in DMSO catalyzed by Cu/Me_6TREN (Me_6TREN = tris(2-(dimethylamino)ethyl)amine) complexes. The contributions are determined using a combination of experimental and simulation techniques.

Scheme 2. Proposed Activator (Re)Generation Pathways in PhotoATRP[a]

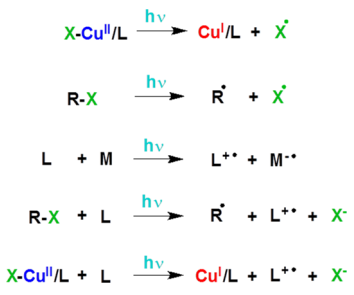

[a]Top is direct reduction of X-Cu^{II}/L, middle are the generation of radicals by the reactions of an alkyl halide and/or a ligand, and bottom is the photochemical reduction of Cu^{II} by an electron donor.

RESULTS AND DISCUSSION

Photochemical Characterization and Polymerization Kinetics. To confirm the significance of the photochemical processes, the kinetics of the same reaction were monitored both with and without light. As illustrated in Figure S1a, the polymerization proceeds efficiently in the presence of light, while in the absence of light the reaction is significantly retarded and is almost non-existent. However, if this same reaction is re-exposed to light, it progresses again and leads to relatively rapid polymerization. This cycle can be repeated multiple times. Figure S1b indicates that the control over the polymer architecture is very good, even with the intermittent cycles of light irradiation and darkness. The molecular weight is close to the theoretical value at all times, and the dispersities are low, ultimately reaching values below $M_w/M_n < 1.05$.

As in any other light-induced process, it is necessary to characterize the polymerization components photochemically. In the literature, the solvent and monomer alone have shown very little photochemical activity,[19,20] therefore only the alkyl halide initiators, ligand, and $CuBr_2$/ligand complex are expected to participate in photochemical reactions. These species, at the concentrations present in polymerization, were characterized by UV−vis/NIR spectroscopy, as shown in Figure 1. The data in Figure 1 indicate that in the region near 400 nm, the strongest absorbance is due to the $CuBr_2$/Me_6TREN complex, with only very weak absorbance due to the alkyl halides MBP and EBiB, and the ligand Me_6TREN, although the oxidized ligand has a light-yellow color, after it has been exposed to air for a long

dx.doi.org/10.1021/ja506379s | J. Am. Chem. Soc. 2014, 136, 13303−13312

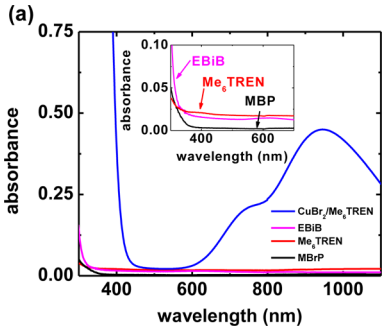

Figure 1. UV−vis/NIR data taken under conditions $[CuBr_2/L] = 0.74$ mM, $[L] = 4.5$ mM, $[EBiB] = [MBP] = 25$ mM, where L= Me_6TREN in MA/DMSO = 2/1 (v/v).

time. In all photochemical processes the first step is the absorbance of the incident photon. In fact, the efficiency of photochemical reactions is not only limited by the intensity of the light source. The absorptivity of the chromophore, the opacity of the secondary reagents, and the quantum yield of the desired pathway are other contributing factors. Quantum yields cannot exceed unity and will not be able to offset the effects of a very low absorbance (such as $A < 0.02$ at 390 nm for Me_6TREN). The involvement of a Cu^{II} chromophore, an open-shell, d^9 transition-metal ion with a rich spectral signature, is much more likely.

In the earliest developments of Cu-mediated photochemical ATRP, the mechanism was proposed to occur by the homolytic cleavage of the Cu^{II}−halogen bond through a ligand to metal charge transfer in the excited state of the X-Cu^{II}/L deactivator complex. This would lead to the formation of a halogen radical and a Cu^{I}/L complex. This pathway is unimolecular and therefore should proceed with no free ligand. Figure S2a gives the polymerization kinetics with a ratio of either $[CuBr_2]$:$[Me_6TREN]$ = 1:1 or 1:6. In the case where $[CuBr_2]$:$[Me_6TREN]$ = 1:1 the concentration of uncoordinated Me_6TREN is very low due to the strong binding between Cu^{II} and Me_6TREN,[38] whereas $[CuBr_2]$:$[Me_6TREN]$ = 1:6 gives 5 equiv of uncoordinated Me_6TREN relative to the $CuBr_2/Me_6TREN$ complex. The kinetics in Figure S2a show virtually no polymerization when all of the ligand was bound to the metal, i.e., $[CuBr_2]$:$[Me_6TREN]$ = 1:1, while a relatively rapid polymerization, reaching over 65% conversion in 6 h, is attained with an excess of ligand, i.e., when $[CuBr_2]$:$[Me_6TREN]$ = 1:6. This indicates that unbound ligand must be involved in the photopolymerization. Figure S2b indicates that the polymers synthesized using an excess of ligand are well controlled with narrow molecular weight distributions. Although it has been reported that excess ligand can reduce end-group fidelity at such low concentration of ligand, it can be reasonably assumed that excess ligand does not decrease end group functionality.

The lack of polymerization with no free ligand also suggests that the unimolecular photochemical reduction of Cu^{II} is kinetically insignificant at 392 nm. These results agree very well with the UV initiated polymerizations performed by Haddleton et al.[20] who also showed that an excess of the ligand is necessary for the photopolymerization to occur under similar conditions.

To confirm that the homolytic cleavage of the Cu^{II} halogen bond is not the key driving force in the photochemical reduction of Cu^{II} to Cu^{I}, a similar polymerization to the one in Figure S2a was performed with copper(II) triflate ($Cu^{II}(OTf)_2$) instead of $CuBr_2$. In both systems the ratio $[Cu^{II}]_0$:$[Me_6TREN]_0$ = 1:6 was used. In the case of the $Cu^{II}(OTf)_2$, there was no added halide salt, so there was no halide binding

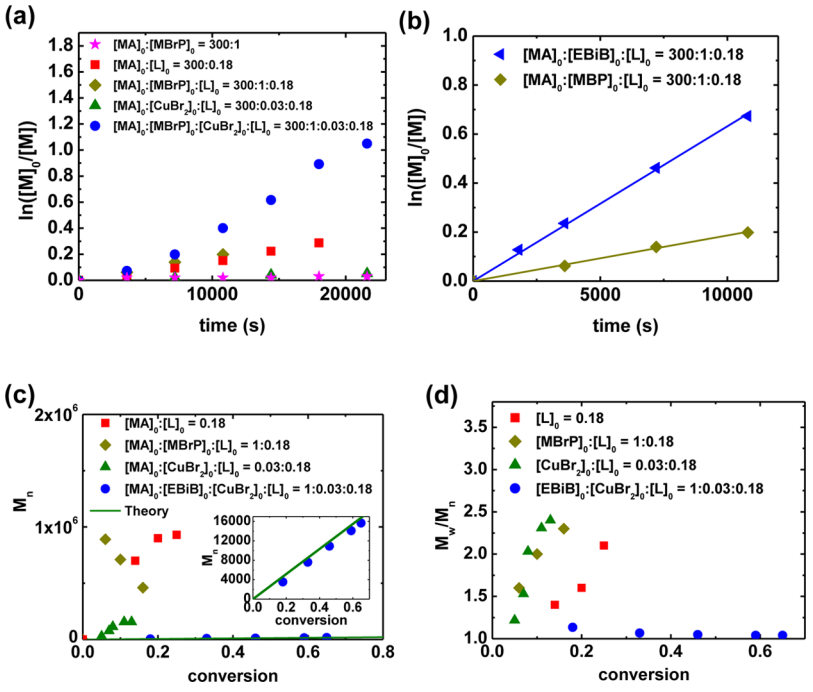

Figure 2. (a) Kinetics and (b) kinetics of RX + L (RX = EBiB or MBP) and (c) evolution of M_n and (d) M_w/M_n with conversion for the various model polymerization of MA in DMSO, with conditions: $[MA]_0$:$[EBiB]_0$:$[CuBr_2]_0$:$[L]_0$ = 300:0−1:0−0.03:0−0.18 with $[MA]_0$ = 7.4 M, 392 nm irradiation (0.9 mW/cm^2) at 25 °C. In all cases the ratios in the caption are relative to $[MA]_0$ = 300. Inset of (c) gives the low molecular weight range of the series (solid blue circle).

dx.doi.org/10.1021/ja506379s | J. Am. Chem. Soc. 2014, 136, 13303−13312

to Cu^{II} at the start of the reaction. Therefore, if the homolytic cleavage of the Cu halogen bond was kinetically significant, the polymerization with the $Cu^{II}(OTf)_2$ should be much slower than the reaction with $Cu^{II}Br_2$. However, as indicated in Figure S3a, the polymerization with $Cu^{II}(OTf)_2$ was initially faster than the reaction with $Cu^{II}Br_2$, clearly indicating that the homolytic cleavage of the Cu^{II}–halogen bond is not kinetically significant.

Figure S3b compares the evolution of molecular weight and the M_w/M_n values with conversion. Both the $Cu^{II}(OTf)_2$ and $Cu^{II}Br_2$ reactions show good agreement between the experimental and theoretical molecular weights, although the M_w/M_n values are higher for the $Cu^{II}(OTf)_2$ system compared to the $Cu^{II}Br_2$ one. The reason for the broader molecular weight distributions in the $Cu^{II}(OTf)_2$ system is that there is initially no deactivator complex in the triflate system. When starting from $Cu^{II}(OTf)_2$, the Br-Cu^{II}/Me_6TREN deactivator complex can only be formed by the loss of bromine from a chain end. This can occur via two pathways. The first is by interaction of an alkyl halide with excess ligand in the presence of light to give an alkyl radical, radical cation and halogen anion, as shown in Scheme 2. This bromide anion can then coordinate with the Cu^{II}/Me_6TREN complex to form the deactivator species. Alternatively, after the photoreduction of Cu^{II}/Me_6TREN in the presence of amines, the generated Cu^{I}/Me_6TREN complex can activate an alkyl halide to give a radical and Br-Cu^{II}/Me_6TREN. This process of deactivator formation is not instantaneous, and therefore, in the initial stages of polymerization, the concentration of deactivator is low which leads to broader molecular weight distributions.

Model Experiments. A series of model experiments were performed to elucidate the polymerization mechanism. These model experiments are similar to the well-controlled polymerization under the conditions: $[MA]_0$:$[EBiB]_0$:$[CuBr_2]_0$:$[Me_6TREN]_0$ = 300:1:0.03:0.18, with $[MA]_0$ = 7.4 M at 25 °C using 392 nm irradiation. The differences are that one or more components are removed from the system to determine the importance/contribution of that component to the overall polymerization. In some cases, the alkyl halide initiator is changed from the more active tertiary EBiB to the less active secondary MBrP.[39] Figure 2a and Table 1 give the kinetics of the polymerization for each model experiment. It is important to note that all of these polymerizations required light, since control experiments performed in the dark yielded no polymer.

MA alone and MA with MBP gave virtually no polymerization, even after 6 h. After the same time, the polymerization mixture containing MA, EBiB, and $CuBr_2$/Me_6TREN and a 5 fold excess of free Me_6TREN to Cu exceeded 60% conversion. The systems containing only MA plus EBiB or MA plus Me_6TREN are fairly slow, reaching just 18% conversion in 3 h and 25% conversion in 5 h, respectively. The Me_6TREN only polymerization is shown in Figure 2a, whereas EBiB polymerization is shown in Figure S4. This indicates that photochemical radical generation from MA alone, Me_6TREN, EBiB, or MBrP is not responsible for the relatively rapid polymerization.

An interesting question arises in the presence of both alkyl halide and amine-based ligands. In the literature, the photochemical radical generation due to alkyl iodide chain ends and amine-based ligands gave rapid and well-controlled polymerization.[24,40] Therefore, either EBiB or MBP was combined with Me_6TREN and monomer to investigate if similar synergies exist between alkyl bromides and amine ligands. As shown in Figure 2b and Table 1, the polymerization with EBiB, Me_6TREN, and monomer was relatively rapid, reaching 49% conversion in 3 h. This rate of polymerization is similar to that of photoATRP. With no Cu assisted activation of alkyl halide, the rate of EBiB groups becoming radical species is very low, and EBiB can remain in the reaction mixture for the whole reaction. However, in the Cu-mediated polymerization, after the initial phase of the reaction the EBiB initiator is converted to the secondary poly(acrylate)-Br chain end, which closely resembles MBP. Therefore, the kinetics of the reaction mixture containing MBP, Me_6TREN, and MA was investigated, as shown in Figure 2a and Table 1. The polymerization containing MBP, Me_6TREN, and MA reached 16% conversion after 1.5 h. In contrast the photoATRP systems that contain Cu species and a similar concentration of alkyl halide and free ligand had a 2–2.5 fold faster polymerization rate.

Table 1. Summary of All Model Experiments Performed under Photochemical Conditions, Using Irradiation at 392 nm[a]

entry	conditions	time (h)	conversion	M_n	M_w/M_n
1	$[MA]_0$:$[EBiB]_0$:$[CuBr_2]_0$:$[L]_0$ = 300:1:0.03:0.18	6	0.65	1.6×10^4	1.04
2	$[MA]_0$:$[EBiB]_0$:$[Cu(OTf)_2]_0$:$[L]_0$ = 300:1:0.03:0.18	6	0.96	2×10^4	1.03
3	$[MA]_0$:$[EBiB]_0$:$[CuBr_2]_0$:$[L]_0$ = 300:0:0:0	6	0.03	–	–
4	$[MA]_0$:$[EBiB]_0$:$[CuBr_2]_0$:$[L]_0$ = 300:0:0:0.18	5	0.25	9×10^5	2.1
5	$[MA]_0$:$[EBiB]_0$:$[CuBr_2]_0$:$[L]_0$ = 300:1:0:0	3	0.18	2×10^6	2.2
6	$[MA]_0$:$[EBiB]_0$:$[CuBr_2]_0$:$[L]_0$ = 300:1:0:0.18	3	0.49	5×10^5	1.9
7	$[MA]_0$:$[MBrP]_0$:$[CuBr_2]_0$:$[L]_0$ = 300:1:0:0	6	0.02	–	–
8	$[MA]_0$:$[MBrP]_0$:$[CuBr_2]_0$:$[L]_0$ = 300:1:0:0.18	1.5	0.16	5×10^5	2.1
9	$[MA]_0$:$[EBiB]_0$:$[CuBr_2]_0$:$[L]_0$ = 300:0:0.03:0.18	6	0.06	4×10^4	1.2
10	$[MA]_0$:$[EBiB]_0$:$[CuBr_2]_0$:$[L]_0$ = 300:0:0.03:0.18	24.25	0.13	2×10^5	2.4
11	$[MA]_0$:$[EBiB]_0$:$[CuBr_2]_0$:$[L]_0$:$[TEA]_0$ = 300:1:0.03:0.03:0.6	6	0.66	2×10^4	1.04

[a]In all cases L refers to Me_6TREN, and all reactions were performed in DMSO with [MA] = 7.4 M.

These results indicate that there is a synergistic radical generation between the secondary poly(acrylate)-like alkyl halide and the ligand. However, this synergy alone is insufficient to explain the relatively rapid polymerization from the standard photoATRP experiment ($[MA]_0$:$[EBiB]_0$:$[Cu^{II}Br_2]_0$:$[L]_0$ = 300:1:0.03:0.18). As highlighted in the Supporting Information, the steady-state rate of photopolymerization was used to determine the apparent rate coefficients of photochemical radical generation from reactions containing individual components (EBiB, MBP, and Me_6TREN) as well as the bimolecular radical generation rate coefficients between both EBiB and Me_6TREN as well as MBP and Me_6TREN. The apparent rate coefficients of radical generation for each component and interaction are given in Table 2. These reactions are essentially photochemically driven ICAR reactions.

Figures 2c and S4 show the evolution of M_n with conversion, and Figure 2d gives M_w/M_n with conversion for all experiments in Table 1. In all cases where Cu was absent, broad molecular

dx.doi.org/10.1021/ja506379s | J. Am. Chem. Soc. 2014, 136, 13303–13312

Table 2. Summary of All Variations of Photochemical Polymerization Conditions, Using Irradiation at 392 nm (0.9 mW/cm^2)[a]

entry	conditions	time (h)	conversion	M_n	M_w/M_n
1	$[MA]_0$:$[EBiB]_0$:$[CuBr_2]_0$:$[L]_0$ = 300:1:0.03:0.18	6	0.65	1.6×10^4	1.04
2	$[MA]_0$:$[EBiB]_0$:$[CuBr_2]_0$:$[L]_0$ = 300:1:0.03:**0.03**	6	0.02	–	–
3	$[MA]_0$:$[EBiB]_0$:$[CuBr_2]_0$:$[L]_0$ = 300:1:0.03:**0.06**	6	0.42	9.5×10^3	1.05
4	$[MA]_0$:$[EBiB]_0$:$[CuBr_2]_0$:$[L]_0$ = 300:1:0.03:**0.12**	6	0.66	1.3×10^4	1.03
5	$[MA]_0$:$[EBiB]_0$:$[CuBr_2]_0$:$[L]_0$ = 300:1:**0.015**:0.165	6	0.63	1.4×10^4	1.05
6	$[MA]_0$:$[EBiB]_0$:$[CuBr_2]_0$:$[L]_0$ = 300:1:**0.006**:0.174	6	0.64	1.3×10^4	1.09
7	$[MA]_0$:$[EBiB]_0$:$[CuBr_2]_0$:$[L]_0$ = 300:**2**:0.03:0.18	6.25	0.74	9.3×10^3	1.04
8	$[MA]_0$:$[EBiB]_0$:$[CuBr_2]_0$:$[L]_0$ = 300:**0.5**:0.03:0.18	6.25	0.57	2.6×10^4	1.02

[a]In all cases L refers to Me_6TREN, and all reactions were performed in DMSO with [MA] = 7.4 M. The parameter being varied from the standard polymerization of entry 1 is highlighted in bold. Polymerizations were stopped between 55–65% conversion to ensure good signal to noise ratio in the NMR signal for estimating monomer conversion. For all molecular weight data, a Mark–Houwink correction was applied, using parameters in the literature.[41] All systems with Cu exhibited molecular weights close to theoretical values within SEC error.

weight distributions were obtained, with $M_w/M_n > 1.5$. Furthermore, in all systems with no Cu, the M_n values were relatively constant and ranging from 5×10^5 to 2×10^6. This indicates that these polymerizations with no Cu in the system have a relatively small number of end groups and that the alkyl halide was not initiating efficiently in the absence of Cu. Based on the molecular weight and conversion data, the radical transfer coefficient for poly(methyl acrylate) to Me_6TREN as well as EBiB was determined, as highlighted in the Supporting Information. The transfer to MBP was assumed to be close to zero, since the molecular weights obtained for the polymerization containing MBP, Me_6TREN, and MA were very similar to the molecular weights obtained for the polymerization containing Me_6TREN and MA only.

The final system investigated as a model reaction contains MA, $CuBr_2$/Me_6TREN, and a 5-fold excess of free Me_6TREN to Cu, but no added alkyl halide. As indicated in Figure 2a and Table 1, this polymerization is relatively slow, reaching only 6% conversion after 6h and 13% conversion after 24.25 h. Figure 2c,d shows the evolution of M_n and M_w/M_n with conversion for the reaction with no added alkyl halide. M_n grows with conversion, although in a non-linear fashion, and the M_w/M_n values were initially low but eventually exceeded 2. This is consistent with previously published data[19] and indicates the formation of new chains after the reduction of Cu^{II} as well as the growth of chains formed earlier in the reaction.

To confirm that the $Cu^{II}Br_2$/Me_6TREN complex is indeed reduced in the presence of an excess of Me_6TREN, the concentration of Cu^{II} was monitored by UV–vis-NIR spectroscopy without added alkyl halides. As shown in Figure S5a,b, the Cu^{II} complex was efficiently reduced in the presence of a 3-fold excess of Me_6TREN to $Cu^{II}Br_2$/Me_6TREN in both pure DMSO and the polymerization medium containing MA and DMSO, with MA/DMSO-2/1 (v/v) [MA] = 7.4 M. However, as shown in Figure S5c,d when all the Me_6TREN was coordinated to Cu, i.e., no free Me_6TREN, virtually no reduction of $Cu^{II}Br_2$/Me_6TREN occurred. The semilogarithmic plots of Cu^{II} photochemically reduced in both DMSO and MA/DMSO are shown in Figure S6. These UV–vis-NIR data in Figure S5 agree well with the polymerization data in Figure S2 and the literature,[20] clearly indicating that the photochemical polymerization and reduction of $Cu^{II}Br_2$/Me_6TREN requires an excess of ligand to proceed.

The model experiments outlined in Figures 2, S3, and S5 suggest that there are two processes of radical generation. The first is analogous to ICAR ATRP and proceeds by the photochemical generation of radicals directly from alkyl halides, amines, or their combined interaction. The second, comparable to ARGET ATRP, includes photochemical reduction of the Cu^{II}/L complexes in the presence of amines which can act as electron donors. The contributions of the ICAR and ARGET processes will be evaluated through simulations later in the manuscript.

An important question that remains after these model experiments is whether the Me_6TREN ligand is unique in its ability to promote photochemical ATRP. To answer this question, a polymerization of MA with EBiB $Cu^{II}Br_2$/Me_6TREN with a 20-fold excess of triethylamine (TEA) to Cu was used instead of 5 equiv of free Me_6TREN. This larger excess of TEA was used to ensure the concentration of tertiary amine groups remained constant. As seen in Figure 3a, the rate

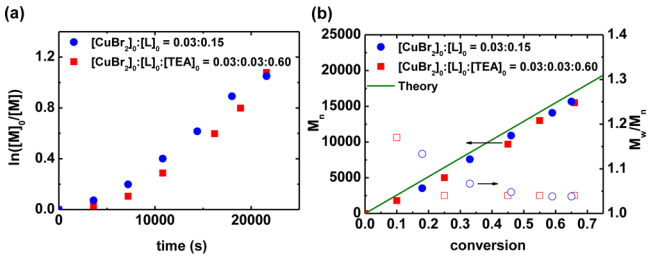

Figure 3. (a) Polymerzation kinetics and (b) evolution of M_n and M_w/M_n with conversion for the polymerization of MA in DMSO under the conditions: $[MA]_0$:$[EBiB]_0$:$[CuBr_2]_0$:$[L]_0$ = 300:1:0.03:0.18 as well as $[MA]_0$:$[EBiB]_0$:$[CuBr_2]_0$:$[L]_0$:$[TEA]_0$ = 300:1:0.03:0.03:0.6 at 25 °C irradiated with 392 nm light (0.9 mW/cm^2).

of the polymerization was virtually the same for Me_6TREN and TEA. This indicates that the rate of the reaction depends only on the concentration of free amine groups in the medium and that an excess of TEA can be used instead of Me_6TREN. Figure 3b compared the evolution of M_n and M_w/M_n with conversion for these two systems. The system with an excess of TEA shows similar control over the polymer architecture and molecular weight distribution as the reaction with an excess of Me_6TREN. This further indicates that the nature of the amine is not important in photochemical ATRP, but instead only the concentration of the aliphatic amine.

Effect of Reaction Conditions on the Photopolymerization. In this section, the effects of reaction conditions, including added ligand, copper, and alkyl halide concentrations were investigated. The reaction conditions are designed such as the other species remain at a constant concentration in order to precisely determine the effect of the reaction parameter on the polymerization. These variations in the reaction conditions help elucidate the mechanism and provide optimal conditions for

dx.doi.org/10.1021/ja506379s | J. Am. Chem. Soc. 2014, 136, 13303–13312

the polymerization. A summary of the experiments performed is given in Table 2.

The first parameter investigated was the concentration of the ligand in the system. Figure 4a shows effect of the ligand

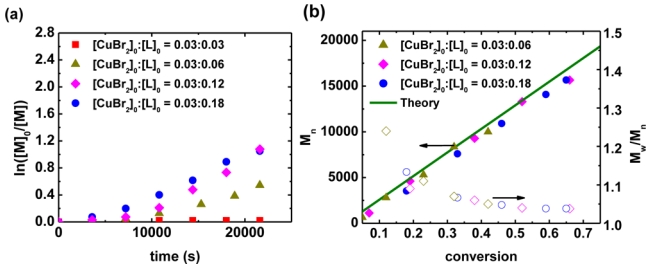

Figure 4. (a) Kinetics and (b) evolution of M_n and M_w/M_n with conversion for polymerization of MA in DMSO under the conditions: $[MA]_0$:$[EBiB]_0$:$[CuBr_2]_0$:$[L]_0$ = 300:1:0.03:0−0.18, [MA] = 7.4 M, irradiated by 392 nm light (0.9 mW/cm^2) at 25 °C.

concentration on the polymerization kinetics. In Figure 4a the concentration of free Me_6TREN was varied from 0 to 5 equiv relative to Cu/Me_6TREN. The system in which no free ligand was present and resulted in no polymerization, while increasing the concentration of ligand lead to an increased rate as illustrated in Figure 4a. These data are consistent with the model experiments in the previous section, which indicated that the uncoordinated ligand is necessary for radical (re)generation. Figure S7 indicates that the steady-state rate of the reaction is proportionational to the square root of the ligand concentration. These square root rate laws are common in ATRP reactions with activator (re)generation being the rate-limiting step.[42,43] Figure 4b displays the evolution of M_n and M_w/M_n with conversion for the polymerizations with different ligand concentrations. Unlike the polymerization rate, the control over the polymer architecture does not depend on the ligand concentration. This is consistent with the idea that the ligand contributes to radical (re)generation, however, once the radical is generated, the Cu^I/Cu^{II}-based ATRP reactions are responsible for deactivating the radical and exchanging it among all the polymer chains.

The second reaction parameter investigated was the concentration of Cu. In these systems, the $Cu^{II}Br_2/Me_6$TREN concentration was varied, keeping the concentration of free ligand equal to 0.15 equiv to the EBiB initiator. In this way, the concentration of the Cu complexes was varied between 20 and 100 ppm with respect to monomer, keeping the absolute concentration of free ligand and alkyl halide constant. As indicated in Figure 5a, the initial concentration of $Cu^{II}Br_2/Me_6$TREN has minimal impact on the rate of the polymerization. This is a surprising result since the reduction of Cu^{II} species is a significant mode of activator (re)generation. Therefore, lower Cu^{II} concentrations should lead to lower rates of polymerization, as has been observed in ARGET ATRP reactions and *e*ATRP processes. The reason for the independence of the polymerization rate on the Cu concentration will be discussed in the subsequent section.

Figure 5b shows the evolution of M_n and M_w/M_n with conversion for the experiments with different concentrations of $Cu^{II}Br_2/Me_6$TREN. The $Cu^{II}Br_2/Me_6$TREN concentration had minimal impact on the evolution of M_n with conversion, since all experimental M_n values agreed well with the theoretical predictions. However, the initial concentration of $Cu^{II}Br_2/$

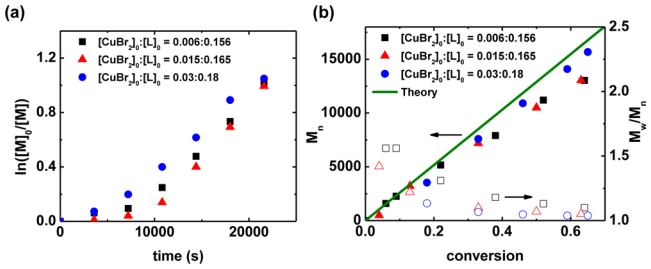

Figure 5. (a) Kinetics and (b) evolution of Mn and M_w/M_n with conversion for polymerization of MA in DMSO under the conditions: $[MA]_0$:$[EBiB]_0$:$[CuBr_2]_0$:$[L]_0$ = 300:1:0.006−0.03:0.156−0.18, [MA] = 7.4 M, irradiated by 392 nm light (0.9 mW/cm^2) at 25 °C.

Me_6TREN had a significant impact on the M_w/M_n values. The narrower molecular weight distributions with higher $Cu^{II}Br_2/Me_6$TREN concentrations are expected, since higher catalyst concentrations lead to shorter transient radical lifetimes, higher rates of radical exchange, and consequently more uniform polymers.

The final reaction parameter investigated was the concentration of the EBiB initiator added to the reaction system. Figure 6a shows the kinetics of polymerization with EBiB

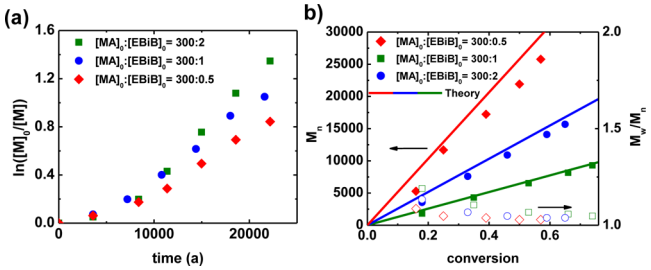

Figure 6. (a) Kinetics and (b) evolution of Mn and M_w/M_n with conversion for polymerization of MA in DMSO under the conditions: $[MA]_0$:$[EBiB]_0$:$[CuBr_2]_0$:$[L]_0$ = 300:0.5−2:0.03:0.18, [MA] = 7.4 M, irradiated by 392 nm light (0.9 mW/cm^2) at 25 °C.

concentrations that target a degree of polymerization (DP) of 150, 300, and 600. Interestingly, the steady-state rate of polymerization increases with increasing alkyl halide concentration. This is an unexpected result because in ATRP processes with activator regeneration such as ICAR or ARGET ATRP, the rate of polymerization is independent of alkyl halide concentration. This is because, at steady state, the concentration of radicals is only dependent on the rate of Cu^I regeneration and the rate of radical termination. In most low copper ATRP processes both of these processes are independent of alkyl halide concentration. Moreover, the photochemical generation of radicals by RX and L is too slow to explain the overall polymerization rate. The dependence of the steady-state polymerization rate is approximately square root in the alkyl halide concentration, as shown in Figure S8. The kinetic analysis and derivation of the mechanism will be developed in the subsequent section. Figure 6b shows the evolution of M_n and M_w/M_n with conversion. As expected, varying the initial EBiB concentration affects the evolution of M_n with conversion, and in all cases the rate of M_n growth is close to the theoretical M_n, determined as the conversion × $[MA]_0/[EBiB]_0$ × M_{MA}, where M_{MA} is the molecular weight of methyl acrylate. Furthermore, the M_w/M_n values depend on the initial concentration of EBiB, with the higher target DPs leading

dx.doi.org/10.1021/ja506379s | J. Am. Chem. Soc. 2014, 136, 13303−13312

to more uniform chains. This observation in Figure 6b is consistent with the typical observations for ATRP with constant deactivator concentrations.[4]

The experiments in Figures 2−6 and Tables 1 and 2 indicate a complex reaction pathway involving several competing pathways to radical (re)generation and radical loss. Therefore, the subsequent sections use the rate coefficients derived from either the literature or model experiments to simulate the photopolymerization. These simulations allow a complete description of the polymerization and allow the contribution of various radical (re)generation pathways to be evaluated.

Simulations of Photochemically Controlled ATRP. Kinetic simulations are a convenient way of assessing the contributions of various reactions to a complex polymerization process. However, these simulations are only indicative of a reaction mechanism if the relevant rate coefficients are well understood. An attractive feature of the polymerization of MA in DMSO, 2/1 (v/v), with Cu/Me_6TREN as the catalyst is that many of the rate coefficients have been reported in the literature.[13] Although certain Cu^I complexes can disproportionate under some reaction conditions,[13,44,45] the recent analysis in the literature indicates that the Cu^IBr/Me_6TREN complex disproportionates very slowly in the polymerization medium of MA/DMSO = 2/1 (v/v) with an excess of ligand and therefore can be neglected.[13] Additionally, the rate of radical (re)generation through photochemical reactions involving alkyl halides, ligands, and Cu^{II} complexes or their combined interaction has been determined, as outlined in the Supporting Information, as well as the rates of radical transfer to the alkyl halides and amine-based ligand. The reactions considered and the associated rate coefficients are given in Table 3.

As mentioned in the text, specific association between the various Cu complexes, halides, and ligands is not explicitly considered, but instead the activity of Cu^I is based on the total Cu^I concentration, and similarly the activity of Cu^{II} is based on the total Cu^{II} concentration. The only exception is when $Cu^{II}(OTf)_2$ is used, since these salts form Cu^{II} complexes without a bound halogen. This Cu^{II}/Me_6TREN complex without a bound halide anion cannot deactivate radicals and is considered as a complex that is distinct from the Cu^{II} deactivator complex.

The photochemical radical (re)generation processes (reactions 14−19) require additional explanation. As listed, small molecule radicals, R•, are generated in each process. For simplicity these species are assumed to have the same reactivity as all other small molecule radicals. However, as will be discussed subsequently, this is an approximation, designed to simplify the simulations, and likely structures of these products will be proposed. Whenever Me_6TREN becomes a radical R•, this radical has a positive charge that is omitted for clarity. Additionally, reactions 16−18 will produce 1 equiv of free bromide anion, however, bromide anion is a spectator in all ATRP reactions and the only situation where this generated bromide can be significant is when $Cu^{II}(OTf)_2$/Me_6TREN is used. In that case, the association to Cu^{II} of the generated bromide in reactions 16−17 was factored into the simulations, and the association is assumed to be very fast. Other things not considered are chain-length-dependent termination.[48,50−52]

In all simulations, the small molecule alkyl halide was chosen to be EBiB or MBP, designed to closely match the experimental conditions. All rate coefficients for reduction were based on an experimentally measured relevant reduction reaction. The rate coefficients: k_{r1EBiB}, k_{r1MBP}, k_{r1L}, $k_{r2EBiB,L}$, and $k_{r2MBP,L}$ were estimated from the polymerization rate of the relevant reaction. The rate coefficient for bimolecular reduction of Cu^{II} species by Me_6TREN, $k_{r2CuBr,L}$, was estimated from the reduction of $CuBr_2$ by an excess of Me_6TREN as shown in Figures 2 and S6. The specific steady-state approximation and formulas used to calculate these rate coefficients can be found in formulas 4−10 in the Supporting Information. It is important to note that the Cu^{II}/Me_6TREN complex without a bound halogen was measured to have a reduction rate 10 times faster than the

Table 3. List of Reactions Relevant to Photochemically-Mediated ATRP Processes

entry	reaction	rate coefficient at 298 K[e]	ref
	ATRP		
1	RBr + $Cu^IBr/L \rightarrow R\bullet + Cu^{II}Br_2/L$	$k_{a1} = 2 \times 10^3$	13,39
2	$R\bullet + Cu^{II}Br_2/L \rightarrow RBr + Cu^IBr/L$	$k_{d1} = 5 \times 10^7$	13,39
3	$P_jBr + Cu^IBr/L \rightarrow P_j\bullet + Cu^{II}Br_2/L$	$k_a = 2 \times 10^2$	13
4	$P_j\bullet + Cu^{II}Br_2/L \rightarrow PBr + Cu^IBr/L$	$k_d = 2.8 \times 10^8$	13
	Radical Propagation		
5	$R\bullet + MA \rightarrow P_1\bullet$	$k_{add,EBiB} = 7.3 \times 10^2$ $k_{add,other} = 1.6 \times 10^4$	46,47
6	$P_j\bullet + MA \rightarrow P_{j+1}\bullet$	$k_p = 1.56 \times 10^4$	46
	Conventional Radical Termination		
7	$R\bullet + R\bullet \rightarrow D_0$	$k_{t0} = 2 \times 10^9$	48
8	$R\bullet + P_j\bullet \rightarrow D_j$	$k_{t0} = 2 \times 10^9$	48
9	$P_j\bullet + P_j\bullet \rightarrow D_{j+k}$	$k_t = 1 \times 10^8$	48
	Catalytic Radical Termination		
10	$R\bullet + Cu^IBr/L \rightarrow D_0 + Cu^IBr/L$	$k_{tx0} = <100$	this work[c]
11	$P_j\bullet + Cu^IBr/L \rightarrow D_j + Cu^IBr/L$	$k_{tx} = 4 \times 10^3$	this work
	Radical Transfer		
12	$P_j\bullet + L \rightarrow D_j + R\bullet$	$k_{tr,L} = 2.8 \times 10^3$	this work
13	$P_j\bullet + RBr \rightarrow D_j + R\bullet$	$k_{tr,EBiB} = 2.3 \times 10^2$	this work[d]
	Photochemical Radical (Re)Generation		
14	$L + MA \rightarrow 2\ R\bullet$	$k_{r2L,M} = 1.5 \times 10^{-9}$	this work
15	$RBr \rightarrow 2\ R\bullet$	$k_{r1EBiB} = 2.9 \times 10^{-9}$ s^{-1}	this work[d]
16	$RBr + L \rightarrow 2\ R\bullet$	$k_{r2EBiB,L} = 6.2 \times 10^{-6}$	this work
17	$RBr + L \rightarrow 2\ R\bullet$	$k_{r2MBP,L} = 1.4 \times 10^{-6}$	this work
18	$Cu^{II}Br_2/L + L \rightarrow Cu^IBr/L + R\bullet$	$k_{r2CuBr,L} = 1 \times 10^{-3}$	this work
19	$Cu^{II}(OTf)_2/L + L \rightarrow Cu^IOTf/L + R\bullet$	$k_{r2CuOTf,L} = 1 \times 10^{-2}$	this work

[a]The value k_{a1} for the α-bromoisobutyrate was taken to be 10 times larger than the value k_a measured for the 2-bromopropionate, which is consistent with the work of Tang et al.[39] [b]The deactivation rate coefficient k_{d1} for the isobutyrate radical was taken to be 6 times smaller than the value k_d measured for the propionate radical, which is consistent with the work of Tang et al.[39] [c]For the reaction of Cu^I-mediated radical loss for tertiary isobutyrate radicals was previously observed to be negligible and therefore taken to be 0.[49] [d]For the reactions of transfer to MBP and PMA-Br the rate coefficient is so low that it could not be determined, therefore was taken to be 0. [e]The units for all rate coefficients are $M^{-1}\ s^{-1}$ unless otherwise noted. [f]In all reactions, L = Me_6TREN.

dx.doi.org/10.1021/ja506379s | J. Am. Chem. Soc. 2014, 136, 13303−13312

Cu^{II}/Me_6TREN with a bound halogen, as seen in Figure S6. This is consistent with the fact that the Br-Cu^{II}/Me_6TREN complex is approximately 250 mV more reducing than the Cu^{II}/Me_6TREN without a bound halogen.[53] The rate of Cu^{I}-mediated radical loss, k_{tx},[49,54] was estimated from the polymerization [MA]:[RX]:[$Cu^{II}Br_2/Me_6TREN$]:[Me_6TREN] = 300:1:0.03:0.15, as outlined in the Supporting Information. This value of k_{tx} = 4000 M^{-1} s^{-1} is lower than that measured in previous work,[49] but this could be due photochemically promoted dissociation of the organometallic P−Cu^{II} intermediate to regenerate Cu^{I} and the radical.

The results of the simulations under conditions that mimic the various model experiments are shown in Figure S9. As expected, the rate of polymerization with MBP was zero, while the system with Me_6TREN only was relatively slow. Similarly, the polymerization rate with $CuBr_2/Me_6TREN$ and an excess of Me_6TREN was very slow, which agrees well with the experimental data. The polymerization rate in the system using MBP and Me_6TREN was faster than the systems with MBP only and Me_6TREN only. These results are broadly consistent with the experiments.

Finally, the polymerizations with the alkyl halide, Cu^{II}, and an excess of ligand were relatively fast. In particular, for the system that started with $CuBr_2$ there was a non-trivial induction period of approximately 2−2.5 h, followed by relatively rapid polymerization. The long induction period is predominantly due to the slow addition of the small molecule isobutyryl radical to the monomer, and it is possible that the true addition rate coefficient is somewhat higher than the one estimated in the literature. Furthermore, the system where $Cu^{II}(OTf)_2$ was used instead of $Cu^{II}Br_2$, the polymerization showed a much shorter induction period (almost none) with very rapid polymerization at the start of the reaction. However, as the reaction proceeded, the polymerization rate decreased toward the rate of polymerization in the system which started with $Cu^{II}Br_2$. In all cases the simulations agree well with the experimental data.

Figure S9b shows the evolution of M_n with conversion. All polymerizations in the absence of Cu species showed high molecular weights, consistent with the experimental data. The simulated evolution of M_n with conversion for the system with $CuBr_2/Me_6TREN$ and an excess of Me_6TREN showed a non-linear, diminishing evolution of M_n with conversion, which is consistent with the experimental data. Finally, the systems with Cu^{II}, alkyl halide and an excess of Me_6TREN showed linear evolution of the simulated molecular weight with good agreement between the simulated and theoretical molecular weights. It is important to note that the triflate system has an initial period with high molecular weights and poor agreement between the theoretical and simulated molecular weight. This is due to inefficient deactivation during the early phase of the reaction, due to a very low concentration of the Cu^{II} deactivator complex.

Figure S9c gives the simulated evolution of M_w/M_n with conversion for the various model experiments and polymerizations. As expected, all polymerizations without Cu give broad molecular weight distributions. The polymerization with only monomer, $CuBr_2/Me_6TREN$, and an excess of Me_6TREN initially gave narrow molecular weight distributions. The higher M_w/M_n values obtained at the end of the reaction can be attributed to the formation of new chains generated by the radical (re)generation processes. The polymerization with alkyl halide, an excess of Me_6TREN, and $Cu^{II}(OTf)_2/Me_6TREN$ initially showed broad molecular weight distributions, due to slow initiation, although these decreased at higher conversion. Finally, the polymerization with alkyl halide, an excess of Me_6TREN, and $Cu^{II}Br_2/Me_6TREN$ showed narrow molecular weight distributions throughout the reaction. These results all agree well with the experimental observations. Finally Figure S9d shows the fraction of living polymer chains. Only the systems which had alkyl halide, ligand, and Cu^{II} added to the system had a high fraction of living chains.

To determine the kinetic contributions of the various reactions to the overall polymerization process, the concentrations of all species in the polymerization, under the conditions: [MA]:[EBiB]:[$Cu^{II}Br_2/Me_6TREN$]:[Me_6TREN] = 300:1:0.03:0.15 were determined. These concentrations are shown in Figure S10a and were subsequently used to determine the rates of the relevant processes. As shown in Figure S10b, the dominant reactions are propagation (R_p) and the ATRP reactions of alkyl halide activation by Cu^{I} (R_a) and radical deactivation by Cu^{II} (R_d). The rates of alkyl halide activation by Cu^{I} and radical deactivation by Cu^{II} are equal from the start of the reaction, implying that the ATRP equilibrium is maintained throughout the reaction. The next most significant reactions are radical loss and radical (re)generation by the reduction of Cu^{II} by ligand. These reactions occur 5 orders of magnitude slower than the ATRP reactions. The next most significant reactions are conventional radical termination and radical (re)generation by the photochemical reaction between the alkyl halide and the ligand. These reactions occur 1 order of magnitude slower than the radical (re)generation by the reduction of Cu^{II} by ligand. Finally the radical (re)generation from the ligand plus monomer is the slowest reaction occurring 2 orders of magnitude slower than the radical (re)generation by the reduction of Cu^{II} by ligand at the start of the reaction, and it decreases with conversion. In Figure S10b, the total rate of radical loss due to both CRT and conventional radical termination is plotted as well as the total rate of radical generation. The radical (re)generation rate is given by $R_{regen} = 2\,R_{r1L} + 2\,R_{r1RX} + 2\,R_{r2RX,L} + 2\,R_{r2Cu,L}$. This accounts for the fact that in all (re)generation processes two radicals are formed or one radical and one Cu^{I}, which can activate an alkyl halide soon after the Cu^{I} is formed, generating a second radical. As can be seen from Figure S10b the rate of radical generation equals the rate of radical termination from about 60% conversion onward. Similar concentration and rate plots are given in Figures S11−S16 for the polymerizations shown in Figure S9. In general, the results are consistent with those in Figure S10, although in most systems there is no ATRP reaction since there is no Cu in the system. The only exception is the reaction starting from $Cu^{II}(OTf)_2$, as shown in Figure S3, which initially has low rates of alkyl halide activation by Cu^{I} and radical deactivation by Cu^{II} for reasons described above. However, this also leads to a low Cu^{I} concentration and suppresses CRT. As the Cu^{II} without halogen is transformed to Cu^{II} with a halogen, the ATRP reactions increase their rate, but also the rate of CRT increases.

The data in Figures 7 and S10b indicate that under polymerization conditions 90% of radical (re)generation is the photochemical reaction between the Cu^{II} complex and the ligand in a reaction similar to ARGET ATRP. Once the Cu^{I} and radical are generated, they enter the ATRP equilibrium. Although these reactions contribute much less, there is also direct radical generation through photochemical reactions involving the alkyl halide or ligand, ca. 1%. The reaction between ligand and macromolecular alkyl halides accounts for

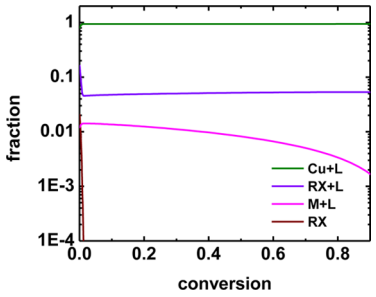

Figure 7. Fraction contributions of activator regeneration from each reaction considered for the simulated polymerization under the conditions, $[MA]_0:[EBiB]_0:[Cu^{II}Br_2/L]_0:[L]_0$ = 300:1:0.03:0.15 in DMSO, [MA] = 7.4 M at 25 °C under 392 nm irradiation (0.9 mW/cm^2). RX is expressed here by a sum of initiating and macromolecular alkyl halides.

8% of activator regeneration. These reactions are essentially photochemical ICAR ATRP reactions.

However, under these polymerization conditions the dominant radical generation mode is the ARGET like process, and the dominant radical loss mode is Cu^I-mediated catalytic radical termination. Therefore, an approximation to the steady-state condition, $2R_{regen} = R_t$ is given below:

$$2k_{r2Cu,L}[Cu^{II}][L] = k_{tx}[Cu^{I}][R^{\bullet}] \quad (20)$$

which can be rewritten to give:

$$[R^{\bullet}] = \frac{2k_{r2Cu,L}[Cu^{II}][L]}{k_{tx}[Cu^{I}]} \quad (21)$$

Since the ATRP equilibrium, $K_{ATRP} = ([R^{\bullet}][Cu^{II}])/([RX][Cu^{I}])$, is maintained through this reaction, the radical concentration can be expressed as follows:

$$[R^{\bullet}] = \sqrt{K_{ATRP}\frac{2k_{r2Cu,L}[L][RX]}{k_{tx}}} \quad (22)$$

This scaling law is consistent with the experiment data in Figures 2, 6, S7, and S8.

Simulations indicate that the mechanism of this Cu-mediated ATRP process is a combination of photochemical ARGET ATRP and photochemical ICAR ATRP. The dominant radical (re)generation reaction is the ARGET like photochemical reduction of Cu^{II} by the excess of amines. Since amines are good electron-donor species, the product is a Cu^I complex and the amine-centered radical cation. After proton abstraction it forms a carbon-centered radical,[37] which reacts with monomer. The overall mechanism consistent with the experimental data is shown in Scheme 4.

CONCLUSIONS

A detailed study of the kinetics of photochemically mediated ATRP in polar media was performed, using 392 nm irradiation. Both experimental and kinetic simulation techniques were used to probe the mechanism of activator and radical (re)generation in the photoATRP process. The results of these experiments and simulations show that the dominant mode of activator (re)generation is the photochemically mediated reduction of Cu^{II} complexes by an excess of amine groups. This is a photochemical ARGET ATRP process, with the amine becoming oxidized to the corresponding radical cation, which can initiate a new chain after proton transfer. The second most

Scheme 4. Proposed Mechanism of Photochemical ATRP[a]

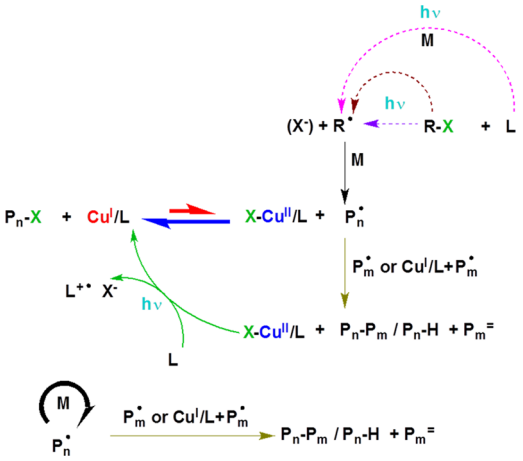

[a]Reactions with the highest rate are in bold, with reactions that dictate the polymerization rate as thin solid lines, and reactions with a small contribution as dashed lines.

significant step is the synergistic radical generation between alkyl halide species and the ligand, which is similar to a photochemical ICAR ATRP. The ICAR-like process occurs approximately 1 order of magnitude slower than the ARGET-like process. Other processes such as direct photochemical cleavage of the alkyl halide, photochemical radical generation from the ligand, or ligand with monomer are minor reactions with very low contribution. The unimolecular reduction of the Cu^{II} deactivator complex does not occur to any appreciable extent. Kinetic simulations revealed that main role of these photochemical reactions is to supplement radicals lost to termination and that control over the polymerization is governed by the classical ATRP activation and deactivation reactions. Thus, photochemically mediated ATRP is a predominantly photochemically mediated ARGET ATRP with contributions from photochemically mediated ICAR ATRP. With the mechanistic insight gained through this study, photochemically mediated ATRP can be used to precisely tune polymer properties for various materials applications.

ASSOCIATED CONTENT

Supporting Information

Details of experimental procedures and additional characterization data. This material is available free of charge via the Internet at http://pubs.acs.org.

AUTHOR INFORMATION

Corresponding Author

km3b@andrew.cmu.edu

Notes

The authors declare no competing financial interest.

ACKNOWLEDGMENTS

NMR instrumentation at CMU was partially supported by NSF (CHE-0130903 and CHE-1039870). We thank the NSF (CHE-1400052) and (CHE-1362629) and members of the CRP consortium for financial assistance.

REFERENCES

(1) Szwarc, M. *Nature* **1956**, *178*, 1168−9.

(2) Moad, G.; Solomon, D. H. *The chemistry of free radical polymerization*, 2nd ed.; Elsevier: Amsterdam, 2006.
(3) Nicolas, J.; Guillaneuf, Y.; Lefay, C.; Bertin, D.; Gigmes, D.; Charleux, B. *Prog. Polym. Sci.* **2013**, *38*, 63−235.
(4) Matyjaszewski, K.; Xia, J. *Chem. Rev.* **2001**, *101*, 2921−2990.
(5) Moad, G.; Rizzardo, E.; Thang, S. H. *Aust. J. Chem.* **2012**, *65*, 985−1076.
(6) Matyjaszewski, K. *Macromolecules* **2012**, *45*, 4015−4039.
(7) Matyjaszewski, K.; Tsarevsky, N. V. *J. Am. Chem. Soc.* **2014**, *136*, 6513−6533.
(8) Fischer, H. *Chem. Rev.* **2001**, *101*, 3581−3610.
(9) Matyjaszewski, K.; Jakubowski, W.; Min, K.; Tang, W.; Huang, J. Y.; Braunecker, W. A.; Tsarevsky, N. V. *Proc. Natl. Acad. Sci. U. S. A.* **2006**, *103*, 15309−15314.
(10) De Paoli, P.; Isse, A. A.; Bortolamei, N.; Gennaro, A. *Chem. Commun.* **2011**, *47*, 3580−3582.
(11) Magenau, A. J. D.; Strandwitz, N. C.; Gennaro, A.; Matyjaszewski, K. *Science* **2011**, *332*, 81−84.
(12) Abreu, C. M. R.; Mendonça, P. V.; Serra, A. n. C.; Popov, A. V.; Matyjaszewski, K.; Guliashvili, T.; Coelho, J. F. J. *ACS Macro Lett.* **2012**, *1*, 1308−1311.
(13) Konkolewicz, D.; Wang, Y.; Zhong, M.; Krys, P.; Isse, A. A.; Gennaro, A.; Matyjaszewski, K. *Macromolecules* **2013**, *46*, 8749−8772.
(14) Guliashvili, T.; Mendonça, P. V.; Serra, A. C.; Popov, A. V.; Coelho, J. F. J. *Chem.—Eur. J.* **2012**, *18*, 4607−4612.
(15) Percec, V.; Guliashvili, T.; Ladislaw, J. S.; Wistrand, A.; Stjerndahl, A.; Sienkowska, M. J.; Monteiro, M. J.; Sahoo, S. *J. Am. Chem. Soc.* **2006**, *128*, 14156−14165.
(16) Tasdelen, M. A.; Uygun, M.; Yagci, Y. *Macromol. Chem. Phys.* **2010**, *211*, 2271−2275.
(17) Tasdelen, M. A.; Uygun, M.; Yagci, Y. *Macromol. Rapid Commun.* **2011**, *32*, 58−62.
(18) Mosnáček, J.; Ilčíková, M. *Macromolecules* **2012**, *45*, 5859−5865.
(19) Konkolewicz, D.; Schröder, K.; Buback, J.; Bernhard, S.; Matyjaszewski, K. *ACS Macro Lett.* **2012**, *1*, 1219−1223.
(20) Anastasaki, A.; Nikolaou, V.; Zhang, Q.; Burns, J.; Samanta, S. R.; Waldron, C.; Haddleton, A. J.; McHale, R.; Fox, D.; Percec, V.; Wilson, P.; Haddleton, D. M. *J. Am. Chem. Soc.* **2014**, *136*, 1141−1149.
(21) Fors, B. P.; Hawker, C. J. *Angew. Chem., Int. Ed.* **2012**, *51*, 8850−8853.
(22) Kwak, Y.; Matyjaszewski, K. *Macromolecules* **2010**, *43*, 5180−5183.
(23) Xu, J.; Jung, K.; Atme, A.; Shanmugam, S.; Boyer, C. *J. Am. Chem. Soc.* **2014**, *136*, 5508−5519.
(24) Ohtsuki, A.; Goto, A.; Kaji, H. *Macromolecules* **2013**, *46*, 96−102.
(25) Treat, N. J.; Fors, B. P.; Kramer, J. W.; Christianson, M.; Chiu, C.-Y.; de Alaniz, J. R.; Hawker, C. J. *ACS Macro Lett.* **2014**, *3*, 580−584.
(26) Anastasaki, A.; Nikolaou, V.; Simula, A.; Godfrey, J.; Li, M.; Nurumbetov, G.; Wilson, P.; Haddleton, D. M. *Macromolecules* **2014**, *47*, 3852−3859.
(27) Alfredo, N. V.; Jalapa, N. E.; Morales, S. L.; Ryabov, A. D.; Le Lagadec, R.; Alexandrova, L. *Macromolecules* **2012**, *45*, 8135−8146.
(28) Xu, J.; Jung, K.; Boyer, C. *Macromolecules* **2014**, *47*, 4217−4229.
(29) Zhang, T.; Chen, T.; Amin, I.; Jordan, R. *Polym. Chem.* **2014**, *5*, 4790−4796.
(30) Xu, J.; Jung, K.; Corrigan, N. A.; Boyer, C. *Chem. Sci.* **2014**, *5*, 3568−3575.
(31) Haddleton, D. M. *Nat. Chem.* **2013**, *5*, 366−368.
(32) Zhou, H.; Johnson, J. A. *Angew. Chem., Int. Ed.* **2013**, *52*, 2235−2238.
(33) McNally, A.; Prier, C. K.; MacMillan, D. W. C. *Science* **2011**, *334*, 1114−1117.
(34) Prier, C. K.; Rankic, D. A.; MacMillan, D. W. C. *Chem. Rev.* **2013**, *113*, 5322−5363.
(35) Wallentin, C.-J.; Nguyen, J. D.; Finkbeiner, P.; Stephenson, C. R. J. *J. Am. Chem. Soc.* **2012**, *134*, 8875−8884.
(36) Klán, P.; Wirz, J. *Photochemistry of Organic Componds: From Concepts to Practice*; John Wiley & Sons: Chippenham, 2009.
(37) Lewis, F. D.; Crompton, E. M. SET Addition of Amines to Alkene. In *CRC Handbook of Organic Photochemistry and Photobiology*, 2nd ed.; Horspool, W. M., Lenci, F., Eds.; CRC Press: Boca Raton, 2010.
(38) Tsarevsky, N. V.; Braunecker, W. A.; Matyjaszewski, K. *J. Organomet. Chem.* **2007**, *692*, 3212−3222.
(39) Tang, W.; Kwak, Y.; Braunecker, W.; Tsarevsky, N. V.; Coote, M. L.; Matyjaszewski, K. *J. Am. Chem. Soc.* **2008**, *130*, 10702−10713.
(40) Goto, A.; Suzuki, T.; Ohfuji, H.; Tanishima, M.; Fukuda, T.; Tsujii, Y.; Kaji, H. *Macromolecules* **2011**, *44*, 8709−8715.
(41) Gruendling, T.; Junkers, T.; Guilhaus, M.; Barner-Kowollik, C. *Macromol. Chem. Phys.* **2010**, *211*, 520−528.
(42) Rosen, B. M.; Percec, V. *Chem. Rev.* **2009**, *109*, 5069−5119.
(43) Tsarevsky, N. V.; Matyjaszewski, K. *Chem. Rev.* **2007**, *107*, 2270−2299.
(44) Rosen, B. M.; Jiang, X.; Wilson, C. J.; Nguyen, N. H.; Monteiro, M. J.; Percec, V. *J. Polym. Sci., Part A: Polym. Chem.* **2009**, *47*, 5606−5628.
(45) Levere, M. E.; Nguyen, N. H.; Leng, X.; Percec, V. *Polym. Chem.* **2013**, *4*, 1635−1647.
(46) Buback, M.; Kurz, C. H.; Schmaltz, C. *Macromol. Chem. Phys.* **1998**, *199*, 1721−1727.
(47) Fischer, H.; Radom, L. *Angew. Chem., Int. Ed.* **2001**, *40*, 1340−1371.
(48) Johnston-Hall, G.; Monteiro, M. J. *J. Polym. Sci., Part A: Polym. Chem.* **2008**, *46*, 3155−3173.
(49) Wang, Y.; Soerensen, N.; Zhong, M.; Schroeder, H.; Buback, M.; Matyjaszewski, K. *Macromolecules* **2013**, *46*, 683−691.
(50) Smith, G. B.; Russell, G. T.; Heuts, J. P. A. *Macromol. Theory Simul.* **2003**, *12*, 299−314.
(51) Heuts, J. P. A.; Russell, G. T.; Smith, G. B.; van Herk, A. M. *Macromol. Symp.* **2007**, *248*, 12−22.
(52) Harrisson, S.; Nicolas, J. *ACS Macro Lett.* **2014**, *3*, 643−647.
(53) Braunecker, W. A.; Tsarevsky, N. V.; Gennaro, A.; Matyjaszewski, K. *Macromolecules* **2009**, *42*, 6348−6360.
(54) Schröder, K.; Konkolewicz, D.; Poli, R.; Matyjaszewski, K. *Organometallics* **2012**, *31*, 7994−7999.